Ocean Modelling 135 (2019) 31–39

Contents lists available at ScienceDirect

Ocean Modelling

journal homepage: www.elsevier.com/locate/ocemod

The perturbation method - A novel large-eddy simulation technique to model realistic turbulence: Application to tidal flow

Ashley Brereton[*,a], Andrés E. Tejada-Martínez[b], Matthew R. Palmer[a], Jeff A. Polton[a]

[a] National Oceanography Centre, Joseph Proudman Building, 6 Brownlow Street, Liverpool, L3 5DA, UK
[b] Civil and Environmental Engineering, University of South Florida, 4202 E. Fowler Ave., Tampa, FL 33620 USA

ARTICLE INFO

Keywords:
Turbulence modelling
Large-eddy simulation
Turbulence closure scheme

ABSTRACT

Turbulence in the ocean dominates the vertical movement of heat and salt, as well as chemical and biological particulates. The modelling of turbulence is therefore essential to forecast the strength of the biological pump, for example, in which CO2 is drawn out of the atmosphere and trapped in the deep ocean. Obtaining observations of turbulence is an expensive process and the modelling of turbulence still remains an open problem. Using state-of-the-art 3D hydrodynamic models, such as Large-Eddy Simulation and Direct Numerical Simulation, to understand turbulence driven by mean flow is a popular method. However in this approach, the turbulence creates its own mean flow contribution which, in some applications, results in an undesirable divergence from the prescribed mean flow. Here, the perturbation method is introduced. This technique ensures zero divergence to the prescribed mean flow. Results reveal the high level of accuracy this approach has in replicating the observed turbulent field when using ADCP mean current data to prescribe the model mean flow. It is envisaged that the user-friendly nature of this method will enable non-specialists to derive turbulence data when turbulence profilers are not a tractable resource. This modelling approach also sets a rigid framework for the testing of turbulence closure schemes.

1. Introduction

Large-eddy simulation (LES) of turbulent flows is used in a wide range of fluid dynamical applications from small scale oceanic dynamics to large scale atmospheric turbulence modelling and many other applications within this scale range (McWilliams et al., 1997; Noh et al., 2004; Moeng, 1984; Kosović and Curry, 2000). The defining characteristic of LES is that small scale fluctuations, which act below the scale of the model resolution - termed as the subgrid-scale (SGS), are parameterised (Smagorinsky, 1963). The resolved scale turbulent fluctuations and mean flow, on the other hand, are calculated directly from the fully 3D Navier–Stokes equations. This method can be very powerful when the majority of the energy containing scales are above the SGS. From this method, computationally expensive turbulent flow solutions can be made much more cost effective with little detriment to the solution. At the current standard of computing resources, LES is becoming a more feasible technique where typically the standard and computationally cheap Reynolds-Averaged-Navier–Stokes (RANS) method is used. However, LES in oceanic turbulence modelling (in contrast to turbulence modelling in the planetary boundary layer), still remains a largely under exploited tool relative to engineering applications.

The main problem in coastal ocean modelling is that the RANS technique is cheap, but it cannot accurately model turbulent fluxes, and the standard LES technique is not feasible for large domains. A growing body of literature is emerging to solve this problem, which combines the two methods. Detached eddy-simulation (Spalart, 2009) where one part of the ocean domain is solved by LES and the other part by RANS. The goal is to use RANS near the wall and LES away from the wall (Zhang et al., 2015) to improve computational cost while retaining reasonable accuracy. Similarly, Chalamalla et al. (2017) develops the so-called SOMAR-LES method, where an LES model is nested inside a parent RANS model (with two-way coupling). This method uses a sophisticated adaptive mesh to track and resolve turbulent fluctuations such that the computational time associated with the LES part is significantly reduced. The LES-coast approach (Roman et al., 2010) is a novel LES technique, whereby the eddy viscosity is split into separate directional components. This allows for an anisotropic domain without an overestimation of the eddy-viscosity and hence allows for a larger grid spacing in the horizontal.

Traditionally, LES in the ocean is used to study effects of surface forcing on the mixed layer (convection, winds, waves etc.) (Vreman

* Corresponding author.
E-mail address: ashbre@noc.ac.uk (A. Brereton).

https://doi.org/10.1016/j.ocemod.2019.01.007
Received 4 June 2018; Received in revised form 5 December 2018; Accepted 17 January 2019
Available online 26 January 2019

et al., 1997; Skyllingstad and Denbo, 1995; Noh et al., 2011), effects of body forcing on the bottom boundary layer (e.g. tidal forcing) (Radhakrishnan and Piomelli, 2008) and effects of these processes in the presence of stratification (Armenio and Sarkar, 2002; Gayen et al., 2010). The reader is directed to Scotti (2010) for an extensive review of the oceanic applications of LES. In some applications, instead of using surface or body forcing, it is more appropriate to prescribe the mean flow when the turbulent properties of the system are of interest. For example, when forcing data is not available, but mean currents are known (Wakata et al., 2017). It is also appropriate to prescribe the mean flow when validating turbulence models (e.g. the $k-\varepsilon$ model Launder and Spalding, 1974) against LES models. This is because the same mean flow can not be achieved by forcing both types of models with the same surface or body forcing, even for simple cases like Couette flow (Coles, 1965). This is undesirable as the ultimate aim is the validate the turbulent characteristics given a particular mean flow. The problem lies in the calculation of the turbulent stresses. Here, the turbulence model and the LES model differ, resulting in mean flow calculations which also differ. However, prescribing the mean flow is not appropriate in many applications, such as assessing boundary layer evolution. For example, bottom boundary layer thickening in the presence of tides and mixed layer deepening in the presence of winds and surface heating. This is because the evolution of the mean flow is what is of interest, something which cannot be investigated when prescribing the mean flow. Furthermore, one cannot fully test the skill of the LES when the mean flow calculation is bypassed. One must first assess the LES's capability to accurately calculate both the mean and turbulent part of the flow field before proceeding with the prescription of a mean flow.

For the cases when prescribing mean flow is appropriate, one problem is apparent. The turbulent fluxes present in the Navier–Stokes equations give rise to an extra (unwanted) mean flow contribution. This term takes the form $<\mathbf{u}'_i\mathbf{u}'_j>$ and symbolizes mean flow generated by the turbulent fluctuations, which is an additional mean flow term, separate to the forcing. If one truly wants to prescribe a mean flow, this extra contribution must be considered. Here, the perturbation method is presented. This method ensures the extra mean flow contribution, which is typically overlooked, is not present. This means that when prescribing the LES with observed mean currents, for example, one can be sure that the turbulence produced is associated purely with the observed mean flow. For the testing of turbulence models against the LES, one can use the perturbation method to ensure both the turbulence model and LES model are forced with the exact mean flow field, giving a higher control over experiments.

This manuscript is set out with the following format. The governing equations for the perturbation method are derived. Given that this method bypasses testing the LES's ability to calculate the mean flow, we devise an experiment: A full (body forced) LES model run is completed, which calculates both mean and turbulent flow fields. The mean flow from this experiment is used to prescribe the perturbation method. The turbulence characteristics are then compared between both methods to show the methods are equivalent in terms of turbulent flow features. This will be followed by an experiment whereby the new method is forced by observed mean currents and the model turbulence data will be compared to observed turbulence data at the same site. Finally, a popular turbulence closure scheme (Canuto et al., 2001) is compared to the perturbation method when both models are forced with the same mean flow forcing from the observational data.

2. Model description

Before the equation set is derived for the turbulent flow, it is convenient to non-dimensionalise all flow variables in the usual way,

$$\boldsymbol{u}=\frac{\boldsymbol{u}^*}{U_0} \qquad \boldsymbol{x}=\frac{\boldsymbol{x}^*}{L} \qquad p=\frac{p^*L}{U_0^2}, \tag{1}$$

where $\boldsymbol{u}=(u,v,w)$ is the non-dimensional form of the flow field, $\boldsymbol{u}^*$ is the dimensional flow field, U_0 is an appropriate velocity scale, $\boldsymbol{x}=(x,y,z)$ is a non-dimensional spatial co-ordinate, $\boldsymbol{x}^*$ is the dimensional co-ordinate, L is an appropriate length scale, p is the non-dimensional pressure and p^* is the dimensional pressure.

The governing (filtered) equations of the total flow field can be described by the Navier–Stokes equations (Stokes, 1845),

$$\frac{\partial\tilde{\boldsymbol{u}}}{\partial t}+\tilde{\boldsymbol{u}}\cdot\nabla\tilde{\boldsymbol{u}}+\frac{1}{Ro}\hat{k}\times\tilde{\boldsymbol{u}}=-\frac{\nabla p}{\rho_0}+\frac{1}{Re}\nabla^2\tilde{\boldsymbol{u}}+\mathrm{SGS}, \tag{2}$$

$$\nabla\cdot\tilde{\boldsymbol{u}}=0, \tag{3}$$

Here, $\tilde{\boldsymbol{u}}$ is the filtered LES resolved velocity field, $Ro=\frac{fL}{U_0}$ is the Rossby number, $Re=\frac{U_0L}{\nu}$ is the Reynolds number, f is the Coriolis parameter, $\hat{k}$ is the unit vector in the vertical and ν is background viscosity. The filter imposed to arrive at Eq. (2), removes all linear dependence on the unresolved flow, $\boldsymbol{u}''$. However, the classic closure problem arises as the filter imposed on the unresolved non-linear term cannot remove dependence on $\boldsymbol{u}''$. This extra contribution by the unresolved flow is encapsulated by the SGS term. To close the equations, typically a Reynolds stress argument is used to relate the unresolved terms to resolvable quantities (Reynolds, 1894). A modelled form of the SGS term is typically of the form:

$$\mathrm{SGS}=2\frac{\partial}{\partial x_j}\left[\frac{\nu_t}{UL}S_{ij}\right] \tag{4}$$

where $S_{ij}=\frac{1}{2}\left(\frac{\partial\tilde{u}_i}{\partial x_j}+\frac{\partial\tilde{u}_j}{\partial x_i}\right)$ is the rate of strain tensor and ν_t is an eddy viscosity. Normally in LES, a variant of the Smagorinsky scheme is used to calculate the eddy-viscosity term e.g. Smagorinsky (1963). Here the formulation for the eddy-viscosity will be taken from Mason and Thomson (1992), which is widely used in the literature (Porté-Agel et al., 2000; Lewis, 2005; Polton et al., 2008)

$$\nu_t=\lambda^2|S| \tag{5}$$

where $|S|=(2S_{ij}S_{ij})^{\frac{1}{2}}$ is the magnitude of the rate of strain tensor, and λ is a length scale defined by,

$$\frac{1}{\lambda}=\frac{1}{\lambda_0}+\frac{1}{\kappa(z+z_0)} \tag{6}$$

where $\lambda_0=C_0\Delta$, C_0 is a constant, taken to be 0.25, $\Delta=(dxdydz)^{\frac{1}{3}}$ is a spatial resolution length scale, Δ^3 is the volume of a grid box, $\kappa=0.4$ is the von Karman constant and z_0 is roughness length prescribed to be 10^{-3}m. Results were found to be insensitive to the values chosen for z_0 and C_0. The first term on the right hand side of Eq. (6) dominates in the interior and the last term dominates near the boundary.

The flow field can be further partitioned into its mean and turbulent constituents akin to Reynolds decomposition (Reynolds, 1894; Tennekes and Lumley, 1972), which comprise the mean and fluctuating parts,

$$\tilde{\boldsymbol{u}}(x,y,z,t)=\boldsymbol{U}(z,t)+\boldsymbol{u}'(x,y,z,t). \tag{7}$$

Here, $\tilde{\boldsymbol{u}}(x,y,z,t)$ is the total flow field, $\boldsymbol{U}(z,t)$ is the mean flow field, $\boldsymbol{u}'(x,y,z,t)$ is the resolved turbulent velocity field, x and y are horizontal axes, z is height above bed and t is time. As one is usually interested in horizontal average quantities to characterise the flow field, it is convenient to define the partitioning in terms of a horizontal average,

$$<\tilde{\boldsymbol{u}}>=\boldsymbol{U}(z,t), \tag{8}$$

such that

$$<\boldsymbol{u}'>=0, \tag{9}$$

where $<\cdot>$ is a horizontal mean defined by,

$$<\cdot>=\frac{1}{XY}\int_x\int_y dxdy \tag{10}$$

where XY is the horizontal area of the domain's extent. It is important to note that the flow field can theoretically be decomposed in any way, so long as the averaging operation $< \cdot >$ is defined consistently with the decomposition.

2.1. The perturbation equations

Our objective is to solve the turbulent constituent of the flow field only. This can be achieved by subtracting the equation for the horizontally averaged flow field, given by:

$$\frac{\partial \boldsymbol{U}}{\partial t} + \boldsymbol{U}\cdot\nabla\boldsymbol{U} + \frac{1}{Ro}\times\boldsymbol{U} + <\boldsymbol{u}'\cdot\nabla\boldsymbol{u}'> = -\frac{\nabla P}{\rho_0} + \frac{1}{Re}\nabla^2\boldsymbol{U} + <SGS>, \tag{11}$$

$$\nabla\cdot\boldsymbol{U} = 0 \tag{12}$$

from Eqs. (2) and (3), respectively, to yield equations:

$$\frac{\partial \boldsymbol{u}'}{\partial t} + \boldsymbol{U}\cdot\nabla\boldsymbol{u}' + w'\frac{\partial \boldsymbol{U}}{\partial z} + \boldsymbol{u}'\cdot\nabla\boldsymbol{u}' - <\boldsymbol{u}'\cdot\nabla\boldsymbol{u}'> + \frac{1}{Ro}\hat{k}\times\boldsymbol{u}' = -\frac{\nabla p'}{\rho_0} + \frac{1}{Re}\nabla^2\boldsymbol{u}' + (SGS - <SGS>). \tag{13}$$

$$\nabla\cdot\boldsymbol{u}' = 0 \tag{14}$$

Here, the first term on the left hand side of Eq. (13) represents time evolution of the turbulence and the second term represents advection of the turbulent field by the prescribed mean flow. The third term represents the injection of turbulent momentum by the velocity shear. The fourth term represents the non-linear advection term and the fifth term is the mean part of the fourth term, which acts to ensure that no extra contribution to the mean flow can arise. The sixth term is a planetary rotation term. On the right hand side of Eq. (13) the first term represents a perturbation pressure gradient, the second term represents diffusion of the turbulent field, the third term represents density perturbations and finally the last term is an eddy viscosity model calculated by means of a Smagorinsky scheme, which is described in the previous section. These equations are similar to that of the DNS study of (Sakamoto and Akitomo, 2008), with the main difference being the inclusion of the fifth term on the LHS of Eq. (13) whereas Sakamoto and Akitomo (2008) omits this term.

A convenient aspect of the two terms which include the horizontal average operator is that their only purpose is to remove the mean part arising in their counterpart term e.g. the fifth term removes the mean part of the fourth term. It can be shown that the only purpose of these two terms is to ensure

$$< \frac{\partial \boldsymbol{u}'}{\partial t} > = 0, \tag{15}$$

which can be demonstrated by applying the horizontal average operator to Eq. (13). This means that, instead of explicitly including the angle bracket terms, one can simply remove the mean part which arises in the first term of Eq. (13), i.e. ensuring that Eq. (15) is satisfied. This also has the advantage of correcting any spurious mean flow (e.g. from numerical diffusion), that might arise as a result of the time-stepping scheme or the grid discretisation scheme implemented. In this way, one can be certain that the mean flow is truly clamped to the input mean flow. This also has the advantage of being much simpler to implement into an existing LES code.

3. Experiment 1 - Validation of the perturbation method

3.1. Experiment design

To validate the implementation of the new model equations, they are first tested against an analogous traditional forcing method setup. Traditional LES methods usually incorporate a two-way interaction between the mean and turbulent constituents of the flow. The proposed perturbation model equations assume a one-way interaction, where the mean flow forces the turbulence and not vice-versa. The assumption of this one-way interaction is that the mean field and the turbulent field are in statistical balance. Therefore, an appropriate experiment will involve using a steady-state setup in the traditional pressure forced LES model i.e. where the mean flow and the turbulent flow are statistically stationary. This will ensure that the mean flow remains unperturbed by the turbulent field in both methods.

3.2. Traditional pressure forced method

The traditional pressure forced method solves the filtered Navier–Stokes equations given by Eq. (2), but with the inclusion of an additional pressure term, which is a source of momentum, given by

$$\frac{\partial \boldsymbol{u}}{\partial t} + \boldsymbol{u}\cdot\nabla\boldsymbol{u} + \frac{1}{Ro}\hat{k}\times w = -\frac{\nabla p}{\rho_0} - \frac{\nabla P}{\rho_0} + \frac{1}{Re}\nabla^2\boldsymbol{u} + \mathrm{SGS}, \tag{16}$$

where

$$-\frac{\nabla P}{\rho_0} \tag{17}$$

is the additional pressure gradient acting as a body force on the flow field. The dynamic Smagorinsky model was used for the SGS term for this experiment (Porté-Agel et al., 2000).

3.2.1. Boundary conditions and numerical configuration

For the purposes of this set up, and to ensure steady-state, $-\frac{\nabla P}{\rho_0} = (0, C, 0)$, where $C = 5\times10^{-4}$ is constant in space and time. Without loss of generality, this pressure forcing will act only in the y-direction. The numerical grid will consist of $64\times64\times96$ points over a (non-dimensional) domain of size of $4\pi\times\frac{16\pi}{3}\times2$ in (x, y, z) directions respectively. No rotation is permitted ($\frac{1}{Ro} = 0$). A bulk Reynolds number of $Re = 5000$ is used and the simulation performed is classified by a friction Reynolds number of $Re_\tau = 160$. To aid in physical interpretation, results will be displayed in dimensional units, with a typical velocity and length scale of $U_0 = 0.1\ \mathrm{ms}^{-1}$ and $L = 25$ m, implying a background viscosity of $\nu = 5\times10^{-4}\ \mathrm{m^2s^{-1}}$. The simulation reached steady state with a mean flow profile shown in Fig. 1(a) and mean shear profile shown in Fig. 1(b). This mean flow and mean shear will be used to force the perturbation method described by Eq. (13). Here, a free-slip condition will be applied to the surface, which will be in direct contrast to the no-slip applied to the surface of the perturbation method due to stability reasons. This difference will be shown to have no discernible effect away from the surface, a desirable quality.

3.3. Results

There are many quantities one can derive to compare properties of each turbulent flow field. However, only important quantities which characterize the amount of energy and transport in the flow namely resolved Reynolds stresses, turbulent kinetic energy (TKE) and energy lost through dissipation (ε) will be compared. Note that all profiles shown in this section have been averaged over the horizontal domain and have been temporally averaged over 1400 time units, once steady-state has been reached (after 1500 simulation time units). To note, it was found that the perturbation method was more stable in terms of the model time-step, allowing a time-step 2.5 times larger. It also took noticeably less time to reach steady-state.

Fig. 2(a) shows Reynolds stress quantities $< u'w' >$ and $< v'w' >$ which describe the vertical fluxes of horizontal momentum. Though the profiles do not match exactly, the difference is not particularly discernible. This would indicate that should a tracer be included in each model, then the vertical transport would be near identical in both cases. This is, for example, important when considering transport of

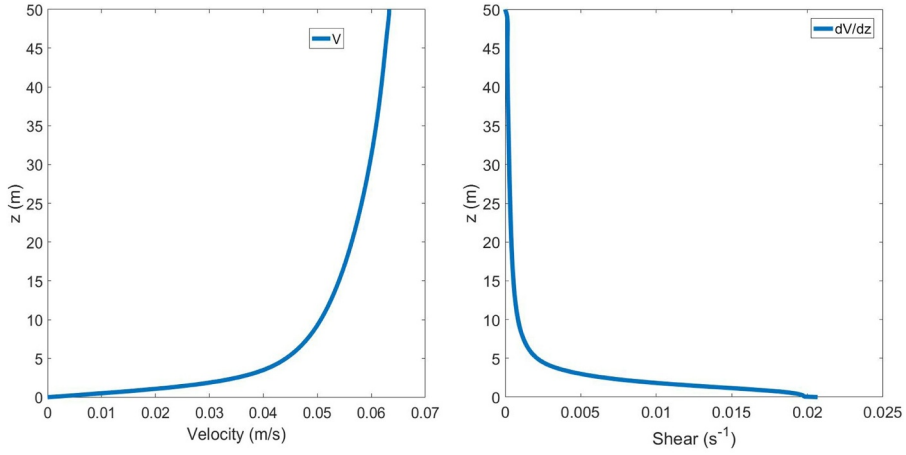

(a) Mean flow (b) Mean shear

Fig. 1. Mean flow and mean velocity shear in the direction of the pressure forcing (along y-axis) calculated from the traditional pressure forced LES method. Mean flow and mean velocity shear in the x-direction is near zero and hence has been omitted from the diagram.

temperature and salinity. Fig. 2(b) shows the components of turbulent kinetic energy, in the form of velocity variances $< u'^2 >$, $< v'^2 >$ and $< w'^2 >$. As the forcing is acting in the y direction, $< v'^2 >$ contains the majority of the energy. It is clear that both models are indistinguishable in the majority of the water column. Notably, the difference only occurs in the local vicinity of the surface. Finally, energy dissipation rate, ε and TKE, defined by;

$$\varepsilon = <(\nu + \nu_t)\frac{\partial u_i'}{\partial x_j}\frac{\partial u_i'}{\partial x_j}> . \qquad TKE = 0.5 \times (<u'^2> + <v'^2> + <w'^2>) \tag{18}$$

are shown in Fig. 3. These profiles are near identical, again, only diverging in the local vicinity of the surface boundary. This is most important as these two metrics are generally used to characterize the turbulence of the flow field. As both models give the same values in the majority of the water column, one can be confident that the difference in surface boundary conditions gives no detrimental effect.

4. Experiment 2 - Forcing by observations

Here, the skill of the perturbation method is assessed via a simple test. Observed mean flow will be processed and used to drive the perturbation equations (Eq. (9)). The resulting modelled turbulent field will be compared to that of the observed turbulent field.

Observations of mean flow were provided by an acoustic Doppler current profiler (ADCP) Lu and Lueck (1999) mounted within the hull of the research vessel. The ADCP delivers high-resolution vertical profiles of horizontal current velocity over the majority of the water column, from approximately 7 m depth to within 3 m of the seabed. Data was collected in an energetic, tidally forced site in Liverpool Bay, UK. This site undergoes significant semi-diurnal tides with a maximum range in excess of 10 m. Very near to the coast Liverpool bay does undergo periodic stratification due to advecting salinity gradients, however the site chosen was suitably offshore to be vertically well mixed throughout this experiment. Hourly CTD surveys confirm that the water column was well mixed. Data was collected on the RV Prince Madog on 10th May 2009, between 07:01 and 19:30 UTC at 10 min intervals. The vessel was anchored at 53° 37.2' N, 3° 55.2' W in 43.1 m of water. The depth averaged mean flow was then derived and used to drive the perturbation equations (Eq. (9)), which were in turn used to generate the model turbulent field.

The observed turbulent field was provided by measurements of the dissipation rate of turbulent kinetic energy, which was derived from shear microstructure measured using a vertically freefalling MSS profiler (Prandke and Stips, 1998). For this experiment, a guard was used to protect the microstructure probes, which enabled the profiler to

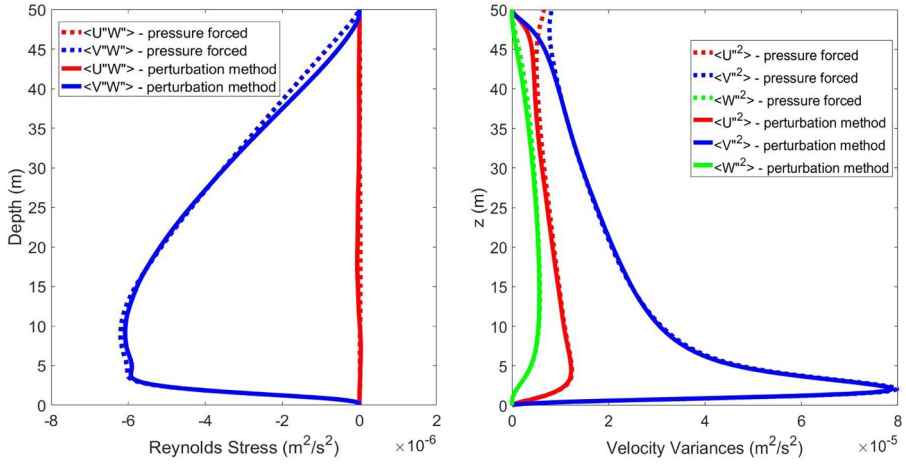

(a) Reynold Stresses (b) Velocity Variances

Fig. 2. Comparison of Reynolds stresses $< u'w' >$ (red) and $< v'w' >$ (blue) alongside a comparison of velocity variance terms $< u'^2 >$ (red), $< v'^2 >$ (blue) and $< w'^2 >$ (green). Each quantity is calculated from the traditional pressure forced method (dashed) and the perturbation method (solid).

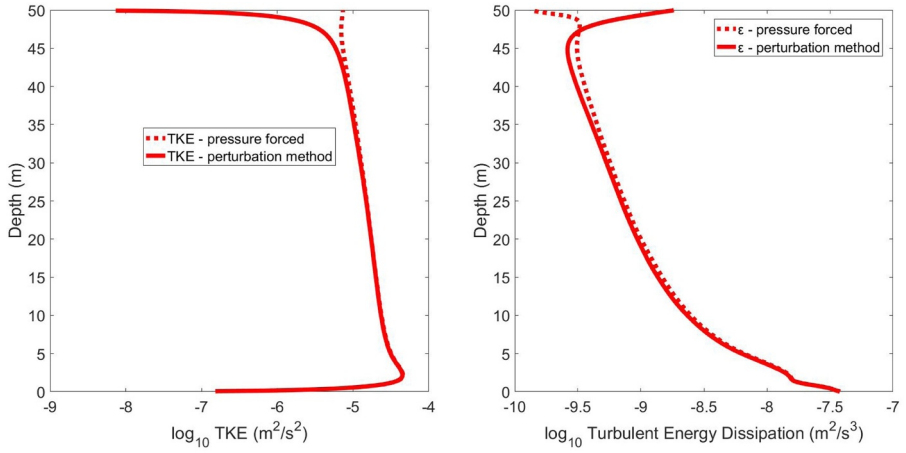

(a) Turbulent kinetic Energy (b) Energy dissipation rate, ε

Fig. 3. A comparison of turbulent kinetic energy (TKE) and energy dissipation rate, ε profiles calculated from the traditional pressure forced method and the perturbation method.

impact the seabed to collect data to within 10cm of the bottom boundary, so resolving the vast majority of turbulence resulting from tidally driven shear.

4.1. Data processing

Due to the formulation of the perturbation equations, mean flow should be a spatial average in the horizontal. However, observations of mean flow are only obtained at one point in the horizontal (lat-lon) field. Therefore the data needs to be appropriately time-averaged. The following assumptions will be enforced. In time, tidal frequencies follow the M2 and M4 harmonics. This will capture the main tidal oscillation and any tidal asymmetries that may arise. In depth, it is assumed that the current profile will match that of the classic log layer, an assumption which is found to be more than reasonable (Jensen et al., 1989). This processed mean flow will then be used to force the perturbation method. The resultant turbulence characteristics (namely energy dissipation rate) from the model simulations will then be compared to observations of energy dissipation rate derived from the microstructure profiler.

To process the ADCP current data to obtain $U(z, t)$ for the perturbation method, an assumption of separability will be used for simplicity i.e.

$$U(z, t) = F(t)G(z), \tag{19}$$

where $F(t)$ will depend on the tidal harmonics and $G(z)$ will depend on a classic log-layer profile. Explicitly, $F(t)$ will take the form:

$$F(t) = \sum_{i=1}^{2} a_i \sin(i\omega t) + b_i \cos(i\omega t), \tag{20}$$

here, $F(t)$ is a Fourier series derived by the least-squares regression method using the deepest observed data, which was 5 m above the bed. As one can see in Fig. 4, this simple expression captures the amplitudes to a high level of accuracy.

The classic log-layer has the form:

$$\frac{u_*}{\kappa} \log\left(\frac{z}{z_0}\right), \tag{21}$$

where κ is the Von Karman constant taken to be 0.4, u_* is the friction velocity at the bed and $z_0 = 10^{-3}$ m is a typical roughness length. To ensure matching of the log-layer to F(t) at the lowest observational point, one arrives at a mean flow of the form:

$$U(z, t) = \frac{F(t)}{\log\left(\frac{5}{z_0}\right)} \log\left(\frac{z}{z_0}\right). \tag{22}$$

Though comparison of this fit with depth at each time will be omitted from this manuscript, it was found to show good agreement to the data at all times. Indeed, the simulated variance in velocity fluctuations (shown later) are an order of magnitude larger than the variance that exists in the deficit between the observed ADCP values and the LES forcing velocities. This suggests that the velocity fitting is not discarding an important source of energy. Furthermore, as commented on earlier, the convenience of this form is that derivatives in z can be taken analytically and interpolation is not needed between observed time points, which increases both accuracy of the solution method and the ease of implementation in the model code.

4.1.1. Boundary conditions and numerical configuration

Velocity and pressure fields were computed from Eq. (13) over a computational domain of 100 m × 100 m horizontally and to a depth of 50 m utilising a grid of 128 × 128 × 192. This implies a resolution scale of $\Delta x = \Delta y \approx 0.8$ m and $\Delta z \approx 0.25$ m, however the grid is stretched to allow higher resolution at the bed, such that $\Delta z = 0.14$ m at the bed and $\Delta z = 0.34$ m at the surface. Horizontal periodicity is enforced at the lateral boundaries and a no-slip condition is imposed on the turbulent flow at the top and bottom. A sponge layer is used in the top 10m, to avoid reflection of energy.

4.2. Results

This section will be devoted to the comparison of the observed and modeled turbulent kinetic energy dissipation rate, denoted by ε_{obs} and ε_{mod} respectively. Provisos need to be taken into account due to the way each variable is calculated, so one should only take a qualitative view on the comparison. Nevertheless, it will still provide a meaningful impression for the skill of the model.

Fig. 5 shows a comparison between ε_{obs} and ε_{mod}. There are two main points about the comparison which are of note. Firstly, the rate at which energy propagates up the water column. The slope of the dashed red line is used to help gauge the upwards propagation rate. One can expect these slopes to depend on the square-root of the eddy-viscosity (Simpson et al., 2000), which indicates that the eddy-viscosity calculated in the SGS scheme is suited for this application. Secondly, ε_{mod} is clearly within a definite order of magnitude compared to ε_{obs}. This can be quantitatively measured by time averaging ε_{obs} and ε_{mod} at each depth bin for each energy plume, shown in Fig. 6. One sees an

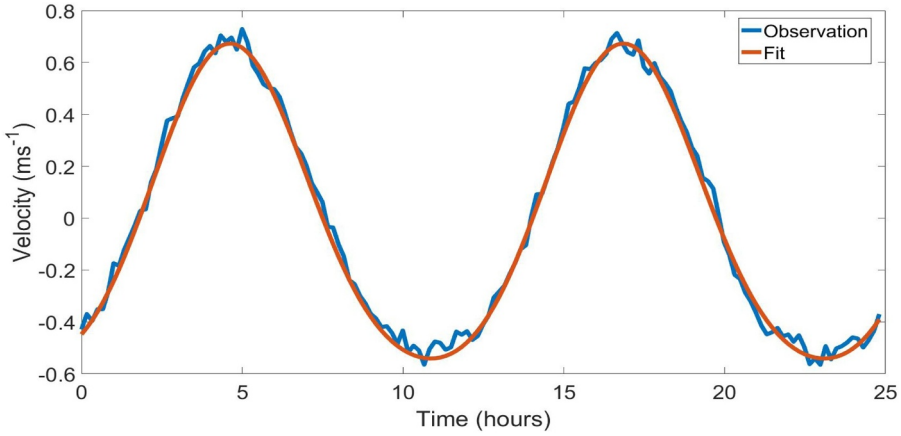

Fig. 4. Near bottom observations (5m from bed) of current velocity directed in the x-direction and the associated Fourier fit.

extremely close fit to the observations, which stay well within an order of magnitude throughout the water column, though there is discrepancy in the second plume in the upper water column. This discrepancy is most likely due to the weak density stratification present in the upper water column, something which is not accounted for in the model.

5. Experiment 3 - Turbulence closure scheme comparison

There is a plethora of different turbulence closure schemes for the RANS equations in the literature (Canuto et al., 2001; Mellor and Yamada, 1982; Cheng et al., 2002). Commonly used in state-of-the-art ocean models are two-equation second-moment closure schemes, which attempt to close unresolved stress quantities such as $< u'w' >$ and $< v'w' >$ in terms of resolved mean quantities i.e.

$$< u'w' > = -\nu_t \frac{\partial U}{\partial z} \qquad < v'w' > = -\nu_t \frac{\partial V}{\partial z} \tag{23}$$

where ν_t is an eddy viscosity derived from an energy and length scale argument, commonly defined by

$$\nu_t = c_\mu \frac{k^2}{\varepsilon} \tag{24}$$

where c_μ is a structure function, generally formulated as a function of stability functions, k is the turbulence kinetic energy and ε is the energy dissipation rate. Two prognostic equations are solved for k and ε for the calculation of ν_t at each model time-step. Note that this is a description of the $k-\varepsilon$ model, popularised by Launder and Spalding (1974) and further developed by various authors (e.g. Shih et al., 1995; Canuto et al., 2001). For a more in depth discussion about $k-\varepsilon$ second-order closure models, see the extensive comparative review of Burchard and Bolding (2001). Other popular models exist, which include the Mellor–Yamada style closure, which derives eddy-viscosity from the prognostic $q^2 - q^2 l$ equations, where q is the turbulence intensity ($q = 2k$) and l is a turbulence length scale (Mellor and Yamada, 1982) and the $k-\omega$ model, where ω is a turbulent frequency scale (Kolmogorov, 1962; Saffman, 1970; Wilcox, 1988). All of these equation sets can be neatly derived as a special case of the generic length scale model (Umlauf and Burchard, 2003), which has been implemented in the General Ocean Turbulence Model (GOTM) (Burchard et al., 1999). The turbulence closure scheme results generated in this work will be derived from model runs using the GOTM software package.

The myriad of closure schemes which are available have been validated by laboratory (Kato and Phillips, 1969; Rohr, 1985; Willis and Deardorff, 1974), DNS (Gerz et al., 1989) and LES (Schumann and Gerz, 1995) experiments. The problem with this is that experiments can not be directly compared to turbulence closure scheme models directly. This is due to the unpredictable mean flow generated by turbulent fluctuations. Furthermore, when density is active, the mean temperature contribution from the density perturbation field also adds an extra degree of freedom in the same way.

Here we present a test case of the popular turbulence closure

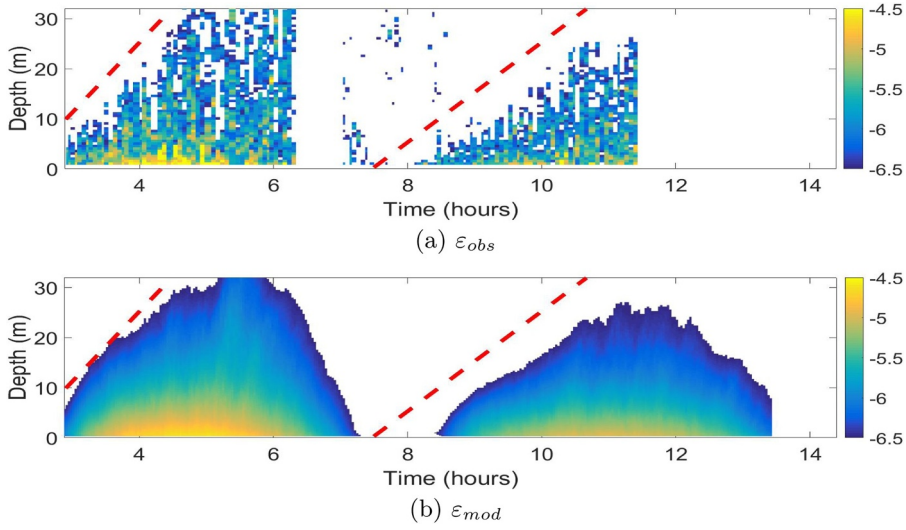

Fig. 5. Comparison of turbulent energy dissipation rate between observations ε_{obs} and the perturbation method ε_{mod}.

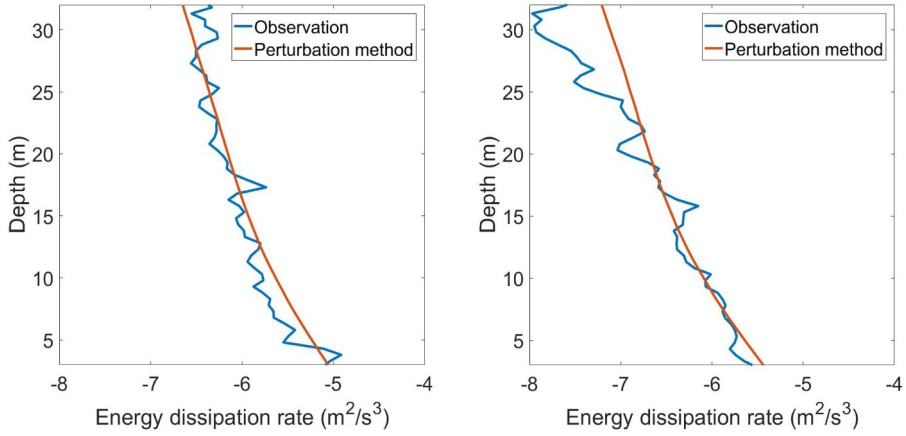

Fig. 6. Comparison of ε_{obs} and ε_{mod} temporally averaged over the first energy plume and second energy plume respectively.

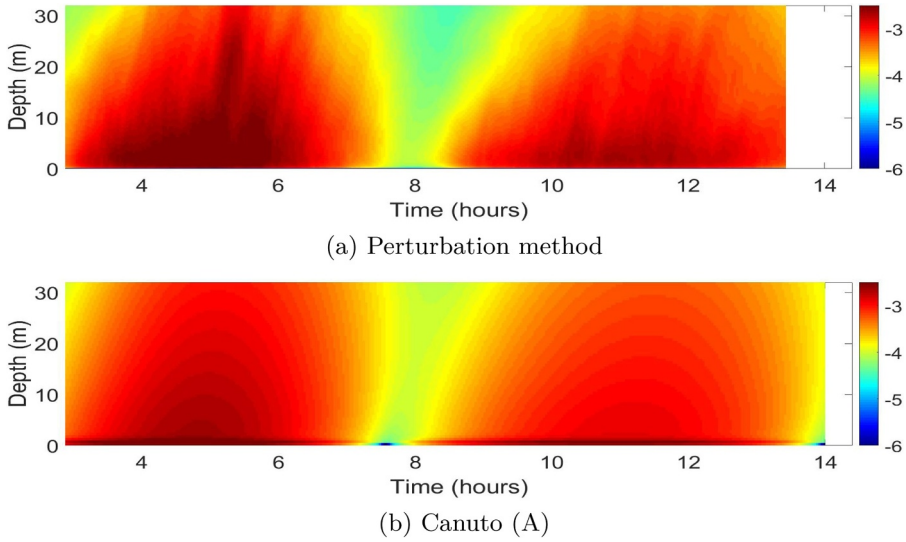

Fig. 7. A comparison of $\log_{10}$ turbulence kinetic energy (m^2s^{-2}) between the perturbation method and the Canuto (A) turbulence model.

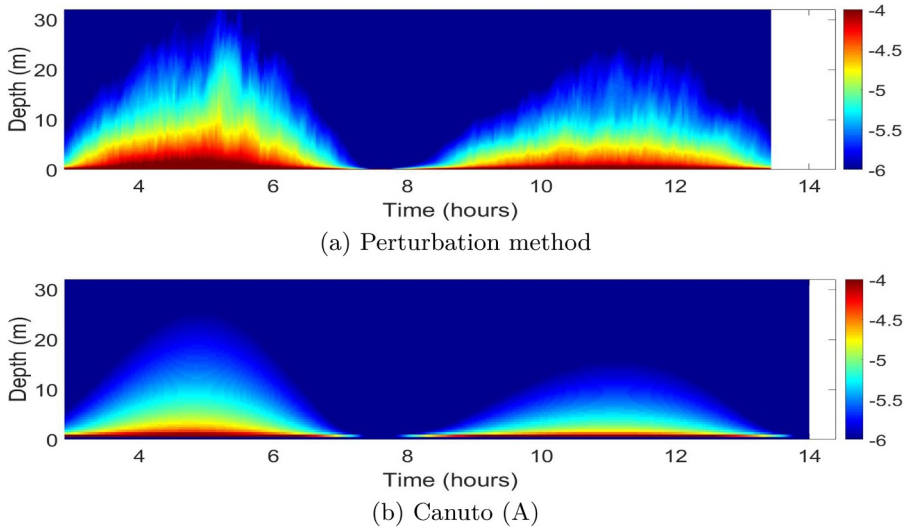

Fig. 8. A comparison of the $\log_{10}$ shear production (m^2s^{-3}) between the perturbation method and the Canuto (A) turbulence model.

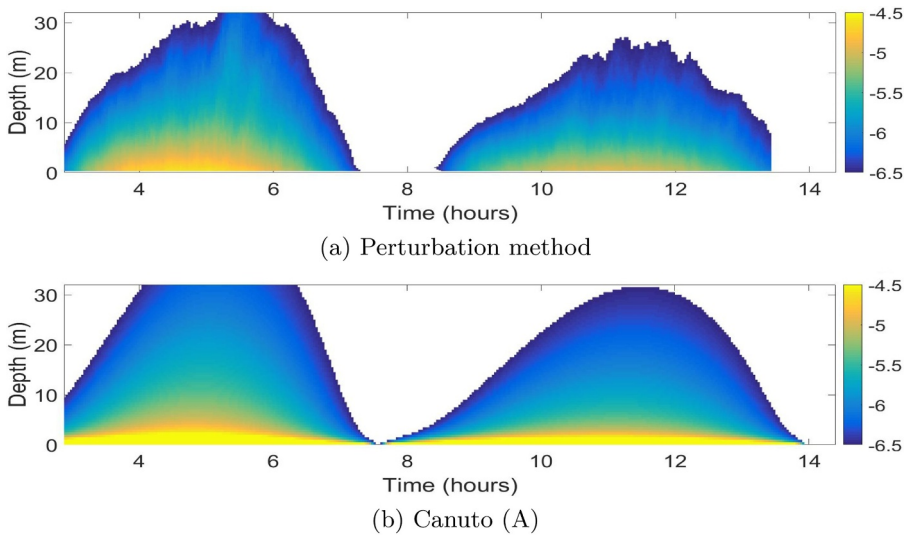

Fig. 9. A comparison of $\log_{10}$ energy dissipation rate (m^2s^{-3}) between the LES model and the Canuto (A) turbulence model.

scheme of (Canuto et al., 2001), denoted by 'Canuto (A)', and its ability to reproduce turbulence data derived by the LES model presented in the previous section. Density stratification will therefore not be considered. For consistency with the perturbation method, a one-way forcing is applied, such that the mean flow is identically Eq. (22). This means that the mean flow will not be solved for in the turbulence closure scheme, only the two prognostic equations for TKE and ε will be solved. This ensures that the forcing which is applied to both models is identical.

5.1. Results

Here, three turbulent statistics will be compared. Energy dissipation rate, TKE and shear production, defined by:

$$< u'w' > \frac{\partial U}{\partial z}, \tag{25}$$

which describes the magnitude of the input of turbulent energy from the tidal shear. It must be stressed that these results are for illustrative purposes only and we make no assertion of the skill of the turbulence closure scheme in question, as to do this, a battery of different experiments must be undertaken.

Fig. 7 shows that the amount of TKE present in Canuto (A) is underestimated compared to the LES. This can be attributed to a lower level of turbulent production, shown here in Fig. 8. As the majority of the shear is produced at the bed, this would imply that the eddy-viscosity near this region is likely to be under estimated. The underestimation of eddy-viscosity has a number of implications. For example, temperature and salinity diffusivity will be lower in the bottom boundary layer, which could possibly result in stratification occurring at the wrong depth. Also, modelling biological or sediment transport with an underestimated eddy-viscosity could change the depth distribution properties. By contrast, the energy dissipation rate shows no similar behavior (Fig. 9). In fact, the results show that energy dissipation is over-estimated. This is surprising, as one would intuitively expect that if TKE was underestimated, then ε would also be underestimated. It does however compound the underestimation of eddy-viscosity (as $\nu_t \propto \frac{k^2}{\varepsilon}$ in the $k-\varepsilon$ model). However, these issues should not detract from the fact that all variables are all well within an order of magnitude of each other, a highly desirable trait.

6. Conclusions

This manuscript presents the perturbation method for LES. The notable characteristics of this method are that the mean flow is explicitly prescribed. Furthermore, in contrast to traditional methods, the turbulent fluxes do not act to diverge the calculated mean flow from the prescribed mean flow. This latter point enables one to have a higher level of control over the model forcing, which is essential for certain applications.

Validation of this technique was completed against a traditional pressure forced large-eddy simulation and the results show clearly that the proposed method works well giving near identical turbulence characteristics away from the surface where the boundary conditions were chosen to differ between methods. Furthermore, using ADCP data from a chosen site in Liverpool Bay, the results demonstrate the high predictive power of the perturbation method in terms of both magnitude and upward transport of energy dissipation rate. Finally, using the same processed ADCP data for forcing, the turbulence closure scheme of (Canuto et al., 2001) was compared against the perturbation method to showcase the application of this new technique.

This method is a strong basis for turbulence closure scheme calibration. Turbulence parameterisations in the presence of stratification is an active area of research (Canuto et al., 2010) but still remains a relatively unsolved problem (Holt and Proctor, 2003; Mahrt, 2014; Scully et al., 2011). Having complete control over the mean shear and stratification means that one can have a greater level of confidence when finding links between the mean and turbulent components of the flow field. Improving turbulence closure schemes using the perturbation method could have implications for many important ocean modelling applications. For example, modelling of the biological pump mechanism, in which planktonic organisms draw CO2 out of the atmosphere and settle it to the deep sea. Also, it could improve estimates of nutrient fluxes through the pycnocline to the surface mixed layer, which is vital for the marine ecosystem population dynamics.

For future work, the perturbation method will be used to examine various scenarios including weakly stratified flows to strong stably stratified flow fields. Using GOTM, a range of different closure schemes will be tested to assess the strengths and weaknesses of each scheme.

Acknowledgement

This work was funded by the UK Natural Research Council under the PycnMix project (NE/L003325/1).

References

Armenio, V., Sarkar, S., 2002. An investigation of stably stratified turbulent channel flow using large-eddy simulation. J. Fluid Mech. 459, 1–42.

Burchard, H., Bolding, K., 2001. Comparative analysis of four second-moment turbulence closure models for the oceanic mixed layer. J. Phys. Oceanogr. 31 (8), 1943–1968.
Burchard, H., Bolding, K., Villarreal, M.R., 1999. GOTM, A General Ocean Turbulence Model: Theory, Implementation and Test Cases. Space Applications Institute.
Canuto, V., Howard, A., Cheng, Y., Muller, C., Leboissetier, A., Jayne, S.R., 2010. Ocean turbulence, iii: new giss vertical mixing scheme. Ocean Modell. 34 (3), 70–91.
Canuto, V.M., Howard, A., Cheng, Y., Dubovikov, M., 2001. Ocean turbulence. part i: one-point closure modelmomentum and heat vertical diffusivities. J. Phys. Oceanogr. 31 (6), 1413–1426.
Chalamalla, V.K., Santilli, E., Scotti, A., Jalali, M., Sarkar, S., 2017. Somar-les: a framework for multi-scale modeling of turbulent stratified oceanic flows. Ocean Modell. 120, 101–119.
Cheng, Y., Canuto, V., Howard, A., 2002. An improved model for the turbulent pbl. J. Atmos. Sci. 59 (9), 1550–1565.
Coles, D., 1965. Transition in circular Couette flow. J. Fluid Mech. 21 (3), 385–425.
Gayen, B., Sarkar, S., Taylor, J.R., 2010. Large eddy simulation of a stratified boundary layer under an oscillatory current. J. Fluid Mech. 643, 233–266.
Gerz, T., Schumann, U., Elghobashi, S., 1989. Direct numerical simulation of stratified homogeneous turbulent shear flows. J. Fluid Mech. 200, 563–594.
Holt, J.T., Proctor, R., 2003. The role of advection in determining the temperature structure of the Irish sea. J. Phys. Oceanogr. 33 (11), 2288–2306.
Jensen, B., Sumer, B., Fredsøe, J., 1989. Turbulent oscillatory boundary layers at high Reynolds numbers. J. Fluid Mech. 206, 265–297.
Kato, H., Phillips, O., 1969. On the penetration of a turbulent layer into stratified fluid. J. Fluid Mech. 37 (4), 643–655.
Kolmogorov, A.N., 1962. A refinement of previous hypotheses concerning the local structure of turbulence in a viscous incompressible fluid at high Reynolds number. J. Fluid Mech. 13 (1), 82–85.
Kosović, B., Curry, J.A., 2000. A large eddy simulation study of a quasi-steady, stably stratified atmospheric boundary layer. J. Atmos. Sci. 57 (8), 1052–1068.
Launder, B.E., Spalding, D.B., 1974. The numerical computation of turbulent flows. Comput. Methods Appl. Mech. Eng. 3 (2), 269–289.
Lewis, D., 2005. A simple model of plankton population dynamics coupled with a les of the surface mixed layer. J. Theor. Biol. 234 (4), 565–591.
Lu, Y., Lueck, R.G., 1999. Using a broadband adcp in a tidal channel. part i: mean flow and shear. J. Atmos. Oceanic Technol. 16 (11), 1556–1567.
Mahrt, L., 2014. Stably stratified atmospheric boundary layers. Annu. Rev. Fluid Mech. 46, 23–45.
Mason, P.J., Thomson, D., 1992. Stochastic backscatter in large-eddy simulations of boundary layers. J. Fluid Mech. 242, 51–78.
McWilliams, J.C., Sullivan, P.P., Moeng, C.-H., 1997. Langmuir turbulence in the ocean. J. Fluid Mech. 334, 1–30.
Mellor, G.L., Yamada, T., 1982. Development of a turbulence closure model for geophysical fluid problems. Rev. Geophys. 20 (4), 851–875.
Moeng, C.-H., 1984. A large-eddy-simulation model for the study of planetary boundary-layer turbulence. J. Atmos. Sci. 41 (13), 2052–2062.
Noh, Y., Goh, G., Raasch, S., 2011. Influence of langmuir circulation on the deepening of the wind-mixed layer. J. Phys. Oceanogr. 41 (3), 472–484.
Noh, Y., Min, H.S., Raasch, S., 2004. Large eddy simulation of the ocean mixed layer: the effects of wave breaking and langmuir circulation. J. Phys. Oceanogr. 34 (4), 720–735.
Polton, J.A., Smith, J.A., MacKinnon, J.A., Tejada-Martínez, A.E., 2008. Rapid generation of high-frequency internal waves beneath a wind and wave forced oceanic surface mixed layer. Geophys. Res. Lett. 35 (13).
Porté-Agel, F., Meneveau, C., Parlange, M.B., 2000. A scale-dependent dynamic model for large-eddy simulation: application to a neutral atmospheric boundary layer. J. Fluid Mech. 415, 261–284.
Prandke, H., Stips, A., 1998. Test measurements with an operational microstructure-turbulence profiler: detection limit of dissipation rates. Aquatic Sci.-Res. Across Boundaries 60 (3), 191–209.
Radhakrishnan, S., Piomelli, U., 2008. Large-eddy simulation of oscillating boundary layers: model comparison and validation. J. Geophys. Res.: Oceans 113 (C2).
Reynolds, O., 1894. On the dynamical theory of incompressible viscous fluids and the determination of the criterion. Proc. R. Soc. London 56 (336–339), 40–45.
Rohr, J. J., 1985. A experimental study of evolving turbulence in uniform mean shear flows with and without stable stratification.
Roman, F., Stipcich, G., Armenio, V., Inghilesi, R., Corsini, S., 2010. Large eddy simulation of mixing in coastal areas. Int. J. Heat Fluid Flow 31 (3), 327–341.
Saffman, P., 1970. A model for inhomogeneous turbulent flow. Proceedings of the Royal Society of London A: Mathematical, Physical and Engineering Sciences. 317. The Royal Society, pp. 417–433.
Sakamoto, K., Akitomo, K., 2008. The tidally induced bottom boundary layer in a rotating frame: similarity of turbulence. J. Fluid Mech. 615, 1–25.
Schumann, U., Gerz, T., 1995. Turbulent mixing in stably stratified shear flows. J. Appl. Meteorol. 34 (1), 33–48.
Scotti, A., 2010. Large eddy simulation in the ocean. Int. J. Comput. Fluid Dyn. 24 (10), 393–406.
Scully, M.E., Geyer, W.R., Trowbridge, J.H., 2011. The influence of stratification and nonlocal turbulent production on estuarine turbulence: an assessment of turbulence closure with field observations. J. Phys. Oceanogr. 41 (1), 166–185.
Shih, T.-H., Liou, W.W., Shabbir, A., Yang, Z., Zhu, J., 1995. A new k-ε eddy viscosity model for high Reynolds number turbulent flows. Comput. Fluids 24 (3), 227–238.
Simpson, J., Rippeth, T., Campbell, A., 2000. The Phase Lag of Turbulent Dissipation in Tidal Flow. Interactions between Estuaries, Coastal Seas and Shelf Seas. Terra Scientific Publishing, Tokyo, Japan, pp. 57–67.
Skyllingstad, E.D., Denbo, D.W., 1995. An ocean large-eddy simulation of Langmuir circulations and convection in the surface mixed layer. J. Geophys. Res.: Oceans 100 (C5), 8501–8522.
Smagorinsky, J., 1963. General circulation experiments with the primitive equations: i. the basic experiment. Mon. Weather Rev. 91 (3), 99–164.
Spalart, P.R., 2009. Detached-eddy simulation. Annu. Rev. Fluid Mech. 41, 181–202.
Stokes, G.G., 1845. On the theories of internal friction of fluids in motion. Trans. Camb. Philos. Soc. 8, 287–305.
Tennekes, H., Lumley, J.L., 1972. A First Course in Turbulence. MIT press.
Umlauf, L., Burchard, H., 2003. A generic length-scale equation for geophysical turbulence models. J. Mar. Res. 61 (2), 235–265.
Vreman, B., Geurts, B., Kuerten, H., 1997. Large-eddy simulation of the turbulent mixing layer. J. Fluid Mech. 339, 357–390.
Wakata, Y., Endoh, T., Yoshikawa, Y., 2017. Les study of near-seabed tide-induced turbulence in the east china sea. Cont. Shelf Res. 145, 21–31.
Wilcox, D.C., 1988. Reassessment of the scale-determining equation for advanced turbulence models. AIAA J. 26 (11), 1299–1310.
Willis, G., Deardorff, J., 1974. A laboratory model of the unstable planetary boundary layer. J. Atmos. Sci. 31 (5), 1297–1307.
Zhang, Y., Habashi, W.G., Khurram, R.A., 2015. Zonal detached-eddy simulation of turbulent unsteady flow over iced airfoils. J. Aircr. 53 (1), 168–181.